

Femtosecond Intersystem Crossing in the DNA Nucleobase Cytosine

Martin Richter,[†] Philipp Marquetand,[‡] Jesús González-Vázquez,[¶] Ignacio Sola,[¶]
and Leticia González*,[‡]

[†]*Institute of Physical Chemistry, Friedrich Schiller University Jena, Helmholtzweg 4, 07743 Jena, Germany*

[‡]*Institute of Theoretical Chemistry, University of Vienna, Währinger Str. 17, 1090 Vienna, Austria*

[¶]*Departamento de Química Física I, Universidad Complutense, 28040 Madrid, Spain*

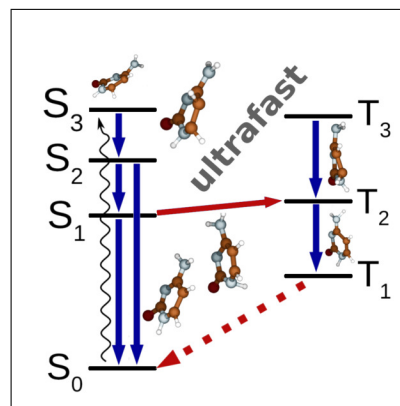
E-mail: leticia.gonzalez@univie.ac.at

Keywords: DNA photostability, excited state dynamics, intersystem crossing, spin-orbit coupling, conical intersection

Abstract

Ab initio molecular dynamics including non-adiabatic and spin-orbit couplings on equal footing is used to unravel the deactivation of cytosine after UV light absorption. Intersystem crossing (ISC) is found to compete directly with internal conversion in tens of femtoseconds, thus making cytosine the organic compound with the fastest triplet population calculated so far. It is found that close degeneracy between singlet and triplet states can more than compensate for very small spin-orbit couplings, leading to efficient ISC. The femtosecond nature of the intersystem crossing process highlights its importance in photochemistry and challenges the conventional view that large singlet-triplet couplings are required for an efficient population flow into triplet states. These findings are important to understand DNA photostability and the photochemistry and dynamics of organic molecules in general.

Graphical TOC Entry



The interaction of DNA and RNA with radiation, from mobile-phone emissions¹ to UV wavelengths,² has enthralled the scientific community for years due to its implications in photodamage.³ Of particular interest is to understand photostability, i.e. the relaxation mechanisms that bring DNA⁴⁻⁶ to the ground state before any other photoreaction can occur. This means that, instead of fluorescence or phosphorescence, the electronic energy provided upon photoexcitation in DNA is transferred to the nuclear degrees of freedom of the molecular system in different ways. It is precisely the atomistic description of these different relaxation pathways that is still heavily discussed in the literature. In the last years it has been clearly established that excited states of isolated DNA nucleobases undergo ultrafast internal conversion (IC) allowing for an efficient radiationless decay towards lower-lying electronic states.⁷⁻¹⁵ The role of intersystem crossing (ISC) in the process of photostability is, however, much less discussed,¹⁵⁻¹⁹ probably because it is thought to be a much slower process in comparison to IC²⁰ and also because the quantum yields of triplet states population in DNA and RNA nucleobases are generally very small and thus difficult to access from the experimental point of view.^{10,15,21} We note, however, that ultrafast time scales for ISC in other organic molecules have been experimentally reported or predicted before.²²⁻³⁶

In this work we present the first excited state dynamical study of a DNA nucleobase including singlet and triplet states. Such simulations are done using the newly developed surface-hopping method SHARC.³⁷ SHARC stands for Surface Hopping including ARbitrary Couplings. With SHARC one can treat non-adiabatic and spin-orbit couplings (which mediate IC and ISC, respectively) on equal footing. The applicability of SHARC to include spin-orbit as well as dipole couplings is documented in Refs.³⁷⁻³⁹ Here, SHARC is employed to investigate the role of the triplet states in the deactivation of cytosine within the framework of nonadiabatic molecular dynamics based on ab initio multi-configurational methods. Such study is necessary to provide a mechanistic insight that

goes beyond what can be learned from quantum chemical calculations alone.

Cytosine presents three tautomers: enol-, keto- and keto-imine-cytosine. Keto-cytosine is the biological relevant tautomer found in the DNA's nucleotides linked to the deoxyribose sugar moiety and the only one for which a crystalline structure exists.⁴⁰ Therefore, here we focus on keto-cytosine. Several stationary points^{3,41,42} of keto-cytosine, including two⁴³⁻⁴⁸ and three-state⁴⁹⁻⁵¹ conical intersections involved in the process of IC have been calculated with ab initio methods. Time-dependent calculations have indicated that the dynamical behavior of cytosine after photoexcitation is one of the most complicated among nucleobases, involving delocalization of the excited wave packet and relaxation through multiple competing pathways in the singlet excited state manifold.^{6,52-54} The possible triplet state formation via ISC along the internal conversion pathway of excited singlet keto-cytosine has been discussed by Merchán et al.^{55,56} in the light of quantum chemical calculations.

Our ab initio molecular dynamic simulations are performed on seven states simultaneously: four singlets and three triplets. Energies, energy gradients, non-adiabatic and spin-orbit couplings are computed on-the-fly using the state-average Complete Active Space Self-Consistent Field (CASSCF) method.^{57,58} Further details are given in the Supporting Information (SI). The first singlet excited state, S_1 , has $\pi\pi^*$ character at the equilibrium geometry and it is bright while the states higher in energy, S_2 and S_3 , correspond to dark $n\pi^*$ excitations, i.e. they have negligible oscillator strengths when vertically excited. The order of states at equilibrium geometry is not altered when going to higher levels of theory that include dynamical correlation (see Table S2 of SI). However, the on-the-fly approach used in this work prohibits the use of higher level methods such as CASPT2 and therefore we employ CASSCF. The Franck-Condon region –from which excitations take place– does not only comprise the equilibrium geometry but also slightly distorted geometries. These distortions are due to the different vibrations included within the zero-

point energy of the system. Because in cytosine rather small deviations of the equilibrium geometry lead to a different ordering of the state character, the S_2 and S_3 states can also be bright states and contribute to the absorption spectrum (see Refs.^{6,53} and Fig. S1 of SI). The character of the lowest three excited triplet states at equilibrium is $\pi\pi^*$ for T_1 and T_2 , and $n\pi^*$ for T_3 . A comprehensive report of vertical excitation energies at different levels of theory can be found in the SI.

In order to obtain a global picture of the relaxation mechanisms of keto-cytosine, we have first used initial conditions spanning the whole first absorption band of the UV spectrum, i.e. covering excitation energies from ca 4 to 7 eV. As explained above, this requires launching trajectories from the first three excited states, S_1 , S_2 and S_3 . Most time-resolved spectroscopic experiments in cytosine^{9,12,48,59,60} use a pumping wavelength of 267 nm (4.64 eV), just below the center of the first absorption band located at 260 nm (4.77 eV). In order to narrow the initial conditions to the energy range corresponding to the experimental one, we have also analyzed the results (Figure S2 of SI) limited to the bandwidth 4.75 ± 0.25 eV, just below our theoretically predicted first absorption band maximum. Also in this energy range, states S_1 to S_3 are excited. The results from both energy ranges qualitatively agree with each other so that we will limit the discussion to the more general broad range.

Figure 1 displays the time evolution of all the state populations and Fig. 2 summarizes the most important deactivation paths found in keto-cytosine with SHARC, including decay times and branching efficiencies. One should note that because the calculations are done at levels of theory which do not include sufficient dynamic correlation, the potential energy surface for the dynamics is not accurate enough to derive quantitative conclusions. Since the energy gaps between the states are highly dependent on the level of theory, the branching efficiencies and the decay times should be considered as an informative basis rather than quantitative numbers. We indicate the *total* branching efficiencies over the whole simulation time so

that in some cases numbers can be higher than the initial population. Percentages not adding to 100% are due to minor pathways not indicated. The decay times are obtained fitting the net amount of hops between two particular states (see Fig. S3 and Table S1 of SI) to an exponential function. The branching efficiencies given in % are also graphically indicated by arrows of different thickness according to their importance. After photo-excitation, which corresponds to time zero in our simulations, the population of the $\pi\pi^*$ is distributed as 13% in S_3 , 47% in S_2 , and 40% in S_1 , as dictated by the weight of the oscillator strength of each state. Since the character of a state can adiabatically change during the simulation, hereafter we shall refer to the states by its energetic order rather than by their character.

Analyzing the 13% population of S_3 , 10% relaxes non-adiabatically to the S_2 and from there to the S_1 within 25 fs. After ca 155 fs, the system populates the electronic ground state S_0 . The remaining 3% of the population of S_3 deactivates directly to S_1 via a threefold degeneracy $S_3/S_2/S_1$, as proposed in Ref.⁵¹ This process is calculated to be slower than the previous one, with a time constant of 110 fs. Most of the population in S_2 transfers preferably to the lower-lying electronic states within less than 100 fs. Also in this case the process of IC is possible via a cascade of subsequent S_2/S_1 and S_1/S_0 conical intersections, or directly via three-state conical intersections $S_2/S_1/S_0$, as proposed in Refs.^{49,51} Both pathways to the ground state are relevant, in agreement with the time-dependent simulations of Ref.⁵³ As deduced from the time constants, the three-state conical intersection pathway is faster (25 fs) than the two-step pathway (25 fs / 155 fs). As noticeable from Fig. 1, the first encounter with a conical intersection takes place within only 10 fs; however, complete depopulation of the S_2 state takes roughly 400 fs. The S_1 state starts with 40% of population. Loss of population is possible via IC to the S_0 state but due to gains from S_2 and S_3 the net effect (see Fig. 1) is that ca 30% of population remains for ca 100 fs, before decaying exponentially to zero in about 0.5 ps.

Conspicuously, due to near degeneracies be-

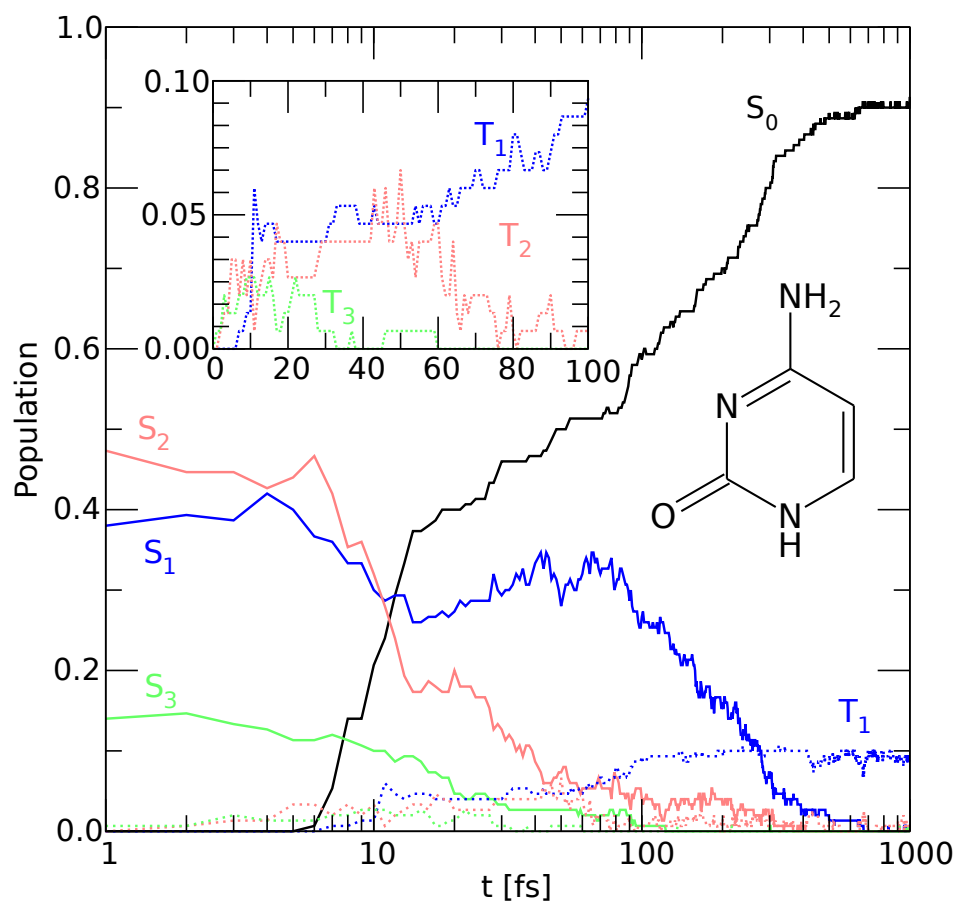


Figure 1: Time evolution of the singlet (solid) and triplet (dotted) states during the first picosecond. The inset zooms the first 100 fs. The S_0 ground state population is in black, S_1/T_1 states populations are in red, S_2/T_2 in blue and S_3/T_3 in green.

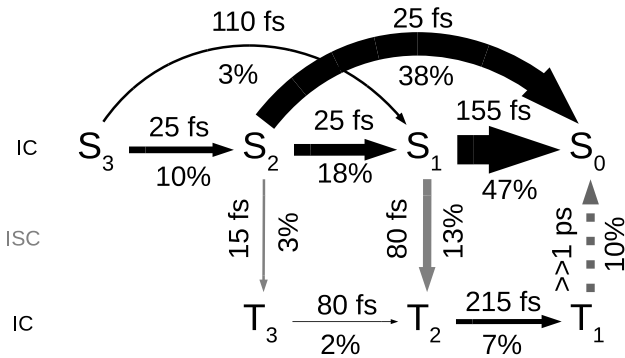


Figure 2: Deactivation pathways of keto-cytosine including internal conversion (IC, in black) and intersystem crossing (ISC, in grey). The propensity of each path is sketched by the thickness of the arrows. The dotted line indicates the deactivation pathway of T_1 .

tween singlet and triplet states, the trajectories clearly show that besides IC, ISC also takes place during the first tens of fs. Triplet states are populated strikingly fast (see inset in Fig. 1). ISC mainly occurs from S_1 to T_2 but in a lesser extent from S_2 to T_3 , see Fig. 2 and Figure S3b in SI. In turn, the trajectories in the T_3 state relax via IC to the T_2 state and those in T_2 quickly convert to T_1 . A minority of the trajectories deactivate directly from T_3 to T_1 via a threefold degeneracy. The simulations show that during the first 20 fs there is a degeneracy of many states (S_0 , S_1 , S_2 , T_1 and T_2), allowing for efficient population transfer. At $t=20$ fs, T_1 and T_2 are populated by ca 5% and T_3 by half of it. The T_3 state is depopulated in less than 100 fs. Most of the population of T_2 has radiationless decayed to T_1 within 200 fs but since it is constantly replenished from S_1 , a small amount of population persists until 1 ps. The trajectories show that as a consequence of the ISC process and the subsequent IC between triplet states, the T_1 state has gained significant population (ca 10%) after 140 fs. This population is stable after the propagation time (1 ps) and most likely can survive during several ps or even ns,⁶⁰ contributing to long-lived transients. The 10% of population trapped in the lowest triplet state agrees with the yield of the dark state ($9\pm 7\%$), from which ISC can take place,

measured by Hare et al.¹⁵

In general, most of the time decay constants calculated are below 100 fs. Ultrafast time-resolved fs pump-probe experiments^{7-12,59,61} for cytosine (and other nucleobases) provide transients with three time scales: one in the fs time regime, $\tau_1 < 100$ fs, and two slower ones, in the ps scale, τ_2 and τ_3 –the latter one even in the ns regime.⁶⁰ As recently noted in Refs.,^{42,48,62} experiments involving ionization integrate over different photoelectron energies or ionic fragments. Interestingly, it has been also demonstrated⁴⁸ that different molecular fragments show different time scales (corresponding to very different relaxation pathways to the ground state). Therefore, the three time constants mentioned above correspond most likely to an average over the many deactivation routes taking place in the nucleobases. As such, our calculated time scales for each of the multitude of relaxation pathways can only contribute to the averaged τ_1 decay time measured in Refs.^{59,60} Sub-picosecond ISC occurring before vibrational relaxation in the S_1 state has been also proposed in DNA base analogues (4-thiothymidine and 6-thioguanosine)^{22-24,63} lending further support to the participation of triplet states in the relaxation process of cytosine. The longest decay time τ_3 can be associated with the ISC from T_1 to the ground state S_0 . Unfortunately, it is difficult to speculate about the origin of the intermediate τ_2 since none of our obtained time scales (recall Figure 2) are in the ps time scale.

Particularly interesting is to note that the obtained ISC mechanism ($S_1 \rightarrow T_2 \rightarrow T_1$) is different from the one previously proposed in the literature, based solely on quantum chemistry. The calculations of Merchán and coworkers⁵⁵ propose $S_1 \rightarrow T_1$ transitions. Their calculations find a minimum in the S_1 potential from where the S_1 and T_1 states are almost degenerate along the minimum energy path. A substantial spin-orbit coupling of 20 - 30 cm^{-1} is found along this path.⁵⁵ In their calculations, the S_1/T_1 crossing corresponds to a transition between the $^1\pi\pi^*$ and the $^3n\pi^*$ states, in agreement with the El-Sayed selection rules for ISC.^{64,65} In contrast, in our calculations,

the ISC takes place fundamentally between the $^1n\pi^*$ (S_1) and the $^3n\pi^*$ (T_2) states, while the $^3\pi\pi^*$ state is the T_1 . Accordingly, and in agreement with the El-Sayed rules, the spin-orbit coupling between S_1 and T_1 is larger (ca 15-20 cm^{-1} in average, maximum 40 cm^{-1}) than between the S_1 and T_2 state (ca 5 cm^{-1} in average). However, the $S_1 \rightarrow T_2$ transition is predominant because the T_2 state is separated from the S_1 by a very small energy gap (< 0.05 eV) for many geometries along the key reaction path. In contrast, the energy gap between the S_1 and T_1 states is at least 0.1 eV for most of the geometries on the same path and hence hopping is not efficient. Clearly, the close degeneracy between the states of different multiplicity can compensate for very small spin-orbit coupling and drive fast ISC, as recently discussed by Worth and coworkers^{34,35} in benzene (see also Ref.⁶⁶). Thus, the $S_1 \rightarrow T_2$ transition dominates the ISC process. This result illustrates the importance of time-dependent dynamical simulations over quantum chemistry calculations alone. In view of our simulations, the S_1 can be considered the precursor state from which the largest ISC takes place before vibrational cooling occurs –as proposed in Ref.¹⁵ or in Refs.^{16,17} for uracil and thymine, respectively.

Another important mechanistic conclusion obtained from the present simulations is that ISC coming from higher states also contributes to the deactivation of keto-cytosine. Common belief is that only spin-flips from the low-lying S_1 state are relevant because ISC transitions in organic molecules without heavy elements are not considered efficient in the fs timescale. Contrary to that, $S_2 \rightarrow T_3$ transitions are possible in keto-cytosine, leading to population transfer of ca 3% after few fs. ISC channels from singlet states higher than the S_1 have been also suggested in e.g. 4-thiothymidine by Reichardt et al.²² or in uracil and thymine by Etinski et al.¹⁹

Further insight into the different competing pathways can be obtained by characterizing the molecular geometries that allow for an efficient population transfer. Figure 3 collects snapshots of archetypal geometries where two or three states are found (near) degenerate (energy less

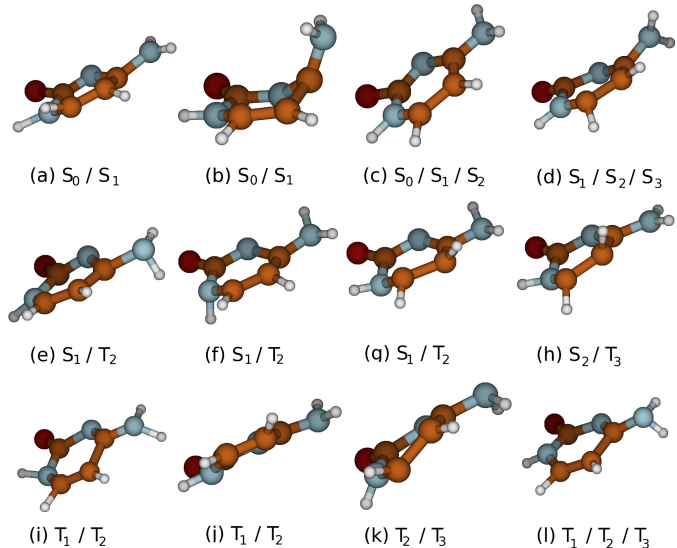


Figure 3: Characteristic geometries displaying near degeneracies between two or three states.

than 0.1 eV). Among the geometries where the S_0 and S_1 states are close in energy, two geometries similar to the twist and sofa S_0/S_1 conical intersections reported by Kotur et al.⁴⁸ could be identified. Figure 3a shows our twist structure, with the carbon atoms twisted by about 70° around the $C=C$ double bond. The sofa conical intersection, Fig. 3b, is characterized by the NH_2 nitrogen displaced from the plane, giving the ring structure the appearance of a sofa. A 3-state near degeneracy between the S_0 , S_1 and S_2 states is a frequent event in keto-cytosine, see Fig. 3c. With the $C=O$ bond elongated to 1.42 Å, the $C=C$ bond between the two CH groups elongated to 1.52 Å, and the NH_2 group pyramidalized to an angle of 45° at the nitrogen, this geometry resembles the structure first optimized by Blancafort et al.⁴⁹ and later on by Kistler and coworkers.⁵¹ Interestingly, this structure is also similar to the semi-planar S_0/S_1 conical intersection published by Barbatti et al.⁵⁴

Figure 3d shows a 3-state degeneracy involving the S_1 , S_2 and S_3 states. Here, the $C=C$ bond is elongated to 1.54 Å and the carbon atoms are twisted about 56° around the $C=C$ double bond. The dihedral at the NH_2 nitrogen is only 22° and therefore, the NH_2 group is rotated by about 35° around the $N-C$ bond rather than pyramidalized. This geometry is differ-

ent from the structures proposed by Kistler et al.⁵¹ The trajectories show that singlet and triplet states are usually near degenerate if the NH₂ group is pyramidalized and starts rotating around the C-N bond, as in Fig. 3e, and/or if the hydrogen of the NH group in para position shows strong out-of-plane oscillations, as in Fig. 3f. Also, when the other hydrogens of the ring show strong out-of-plane movement, near singlet/triplet degeneracies take place, see Figs. 3g,h. To the best of our knowledge no conical intersections between triplet states are reported so far –most likely because only T₁ was believed to be involved in ISC. Figs. 3i,j,k show geometries where two triplet states are degenerate. A degeneracy between T₁ and T₂ (Figs. 3i) occurs when the C-C bond next to the NH₂ group is elongated up to 1.68 Å. Additionally, the NH₂ group is pyramidalised and the hydrogen of the NH group in para position shows out-of-plane movement. Other structures like the one given in Fig. 3j show a twist of the C=C double bond and a slight out-of-plane movement of the whole NH group, leading to a degeneracy of the T₁ and T₂ states. The geometries where T₂ and T₃ come close in energy show similar features: pyramidalisation of the NH₂ group and the out-of-plane movements of the ring hydrogens, see Fig. 3k. Additionally, the C=C double bond is twisted and rotated out-of-plane. Additionally, triple degeneracies of triplet states have been also identified, see Fig. 3l, although they are not operative within 1 ps. Here, the NH₂ group is pyramidalized by 67° and the C-C bond next to the NH₂ group is elongated to 1.71 Å. This indicates that IC from T₃ is not only possible via subsequent T₃/T₂ and T₂/T₁ conical intersections, but also directly from T₃ → T₁.

In summary, our work provides a theoretical rationale for the nuclear factors that make ISC compete with IC in isolated keto-cytosine. As this study demonstrates, the fate of energy relaxation in many complex molecules cannot be revealed by a frozen picture, i.e. quantum chemical calculations at optimized geometries. Instead, a time-dependent picture is necessary, where both IC and ISC compete as dynamical events. ISC is generally quoted in textbooks²⁰

as a slower process in comparison to IC. As a result, many scientists are unaware that ISC can be also an ultrafast process, not only when heavy atoms are present (see e.g.⁶⁷), but also in organic molecules –as this study evidences.

Acknowledgement This work is financed by the Deutsche Forschungsgemeinschaft (DFG) within the project GO 1059/6-1, by the German Federal Ministry of Education and Research within the research initiative PhoNa, the Dirección General de Investigación of Spain under Project No. CTQ2008-06760, a Juan de la Cierva contract, and the European COST Action CM0702. We thank T. Weinacht for helpful discussions regarding cytosine experiments. Generous allocation of computer time in Jena (Computer Center) and Vienna (Vienna Scientific Cluster) is gratefully acknowledged.

Supporting Information Available

Computational details, calculated UV absorption spectra as well as additional results.

References

- (1) Nylund, R.; Leszczynski, D. Mobile Phone Radiation Causes Changes in Gene and Protein Expression in Human Endothelial Cell Lines and the Response Seems to be Genome- and Proteome-Dependent. *Proteomics* **2006**, *6*, 4769–4780.
- (2) Crespo-Hernández, C. E.; Cohen, B.; Kohler, B. Base Stacking Controls Excited-State Dynamics in A-T DNA. *Nature* **2005**, *436*, 1141–1144.
- (3) Shukla, M. K.; Leszczynski, J. Radiation Induced Molecular Phenomena in Nucleic Acids. **2008** (Springer).
- (4) Schultz, T.; Samoylova, E.; Radloff, W.; Hertel, V. I.; Sobolewski, A. L.; Domcke, W. Efficient Deactivation of a Model Base Pair Via Excited-State Hydrogen Transfer. *Science* **2004**, *306*, 1765–1768.

- (5) Abo-Riziq, A.; Grace, L.; Nir, E.; Kabelac, M.; Hobza, P.; Vries, M. S. d. Photochemical Selectivity in Guanine-Cytosine Base-Pair Structures. *Proc. Natl. Acad. Sci. USA* **2005**, *102*, 20–23.
- (6) Barbatti, M.; Aquino, A. J. A.; Szymczak J. J.; Nachtigallová, D.; Hobza, P.; Lischka, H. Relaxation Mechanisms of UV-Photoexcited DNA and RNA Nucleobases. *P. Natl. Acad. Sci. USA* **2010**, *107*, 21453–21458.
- (7) Peon, J.; Zewail, A. H. DNA/RNA Nucleotides and Nucleosides: Direct Measurement of Excited-State Lifetimes by Femtosecond Fluorescence Up-Conversion. *Chem. Phys. Lett.* **2001**, *348*, 255–262.
- (8) Pecourt, J. M. L.; Peon, J.; Kohler, B. Ultrafast Internal Conversion of Electronically Excited RNA and DNA Nucleosides in Water. *J. Am. Chem. Soc.* **2000**, *122*, 9348–9349.
- (9) Kang, H.; Lee, K. T.; Jung, B.; Ko, Y. J.; Kim, S. K. Intrinsic Lifetimes of the Excited State of DNA and RNA Bases. *J. Am. Chem. Soc.* **2002**, *124*, 12958–12959.
- (10) Crespo-Hernández, C. E.; Cohen, B.; Hare, P. M.; Kohler, B. Ultrafast Excited-State Dynamics in Nucleic Acids. *Chem. Rev.* **2004**, *104*, 1977–2020.
- (11) Ullrich, S.; Schultz, T.; Zgierski, M. Z.; Stolow, A. Electronic Relaxation Dynamics in DNA and RNA Bases Studied by Time-Resolved Photoelectron Spectroscopy. *Phys. Chem. Chem. Phys.* **2004**, *6*, 2796–2801.
- (12) Canuel, C.; Mons, M.; Piuzzi, F.; Tardivel, B.; Dimicoli, I.; Elhanine, M. Excited States Dynamics of DNA and RNA Bases: Characterization of a Stepwise Deactivation Pathway in the Gas Phase. *J. Chem. Phys.* **2005**, *122*, 074316.
- (13) Kwok, W. M.; Ma, C.; Phillips, D. L. Femtosecond Time- and Wavelength-Resolved Fluorescence and Absorption Spectroscopic Study of the Excited States of Adenosine and an Adenine Oligomer. *J. Am. Chem. Soc.* **2006**, *128*, 11894–11905.
- (14) Vayá, I.; Gustavsson, T.; Miannay, F. A.; Douki, T.; Markovitsi, D. Fluorescence of Natural DNA: From the Femtosecond to the Nanosecond Time Scales. *J. Am. Chem. Soc.* **2010**, *132*, 11834–11835.
- (15) Hare, P. M.; Crespo-Hernández, C. E.; Kohler, B. Internal Conversion to the Electronic Ground State Occurs via Two Distinct Pathways for Pyrimidine Bases in Aqueous Solution. *P. Natl. Acad. Sci. USA* **2007**, *104*, 435–440.
- (16) Hare, P. M.; Crespo-Hernández, C. E.; Kohler, B. Solvent-Dependent Photophysics of 1-Cyclohexyluracil: Ultrafast Branching in the Initial Bright State Leads Nonradiatively to the Electronic Ground State and a Long-Lived $^1n\pi^*$ State. *J. Phys. Chem. B* **2006**, *110*, 18641–18650.
- (17) Hare, P. M.; Middleton, C. T.; Mertel, K. I.; Herbert, J. M.; Kohler, B. Time-Resolved Infrared Spectroscopy of the Lowest Triplet State of Thymine and Thymidine. *Chem. Phys.* **2008**, *347*, 383–392.
- (18) Kwok, W. M.; Ma, C.; Phillips, D. L. A Doorway State Leads to Photostability or Triplet Photodamage in Thymine DNA. *J. Am. Chem. Soc.* **2008**, *130*, 5131–5139.
- (19) Etinski, M.; Fleig, T.; Marian, C. M. Intersystem Crossing and Characterization of Dark States in the Pyrimidine Nucleobases Uracil, Thymine, and 1-Methylthymine. *J. Phys. Chem. A* **2009**, *113*, 11809–11816.
- (20) McQuarrie, D. A.; Simon, J. D. *Physical Chemistry* **1997** (University Science Books).

- (21) Cadet, J.; Vigny, P. The Photochemistry of Nucleic Acids. *Bioorganic Photochemistry* **1990**, *1*, 1–272.
- (22) Reichardt, C.; Crespo-Hernández, C. E. Room-Temperature Phosphorescence of the DNA Monomer Analogue 4-Thiothymidine in Aqueous Solutions after UVA Excitation. *J. Phys. Chem. Lett.* **2010**, *1*, 2239 – 2243.
- (23) Reichardt, C.; Guo, C.; Crespo-Hernández, C. E. Excited-State Dynamics in 6-Thioguanosine from the Femtosecond to Microsecond Time Scale. *J. Phys. Chem. B* **2011**, *115*, 3263 – 3270.
- (24) Reichardt, C.; Crespo-Hernández, C. E. Ultrafast Spin Crossover in 4-Thiothymidine in an Ionic Liquid. *Chem. Commun.* **2010**, *46*, 5963 – 5965.
- (25) Cavaleri, J. J.; Prater, K.; Bowman, R. M. An Investigation of the Solvent Dependence on the Ultrafast Intersystem Crossing Kinetics of Xanthone. *Chem. Phys. Lett.* **1996**, *259*, 495 – 502.
- (26) Tamai, N.; Asahi, T.; Masuhara, H. Intersystem Crossing of Benzophenone by Femtosecond Transient Grating Spectroscopy. *Chem. Phys. Lett.* **1992**, *198*, 413 – 418.
- (27) Aloise, S.; *et al.* The Benzophenone $S_1(n,\pi^*) \rightarrow T_1(n,\pi^*)$ States Intersystem Crossing Reinvestigated by Ultrafast Absorption Spectroscopy and Multivariate Curve Resolution. *J. Phys. Chem. A* **2008**, *112*, 224–231.
- (28) Zugazagoitia, J. S.; Collado-Fregoso, E.; Plaza-Medina, E. F.; Peon, J. Relaxation in the Triplet Manifold of 1-Nitronaphthalene Observed by Transient Absorption Spectroscopy. *J. Phys. Chem. A* **2009**, *113*, 805–810.
- (29) Ghosh, R.; Palit, D. K. Ultrafast Dynamics of the Excited States of 1-(p-Nitrophenyl)-2-(Hydroxymethyl)Pyrrolidine. *J. Phys. Chem. A* **2012**, *116*, 1993–2005.
- (30) Minns, R. S.; Parker, D. S. N.; Penfold, T. J.; Worth, G. A.; Fielding, H. H. Competing Ultrafast Intersystem Crossing and Internal Conversion in the Channel 3 Region of Benzene. *Phys. Chem. Chem. Phys.* **2010**, *12*, 15607–15615.
- (31) Crespo-Hernández, C. E.; Burdzinski, G.; Arce, R. Environmental Photochemistry of Nitro-PAHs: Direct Observation of Ultrafast Intersystem Crossing in 1-Nitropyrene. *J. Phys. Chem. A* **2008**, *112*, 6313–6319.
- (32) Reichardt, C.; Vogt, R. A.; Crespo-Hernández, C. E. On the Origin of Ultrafast Nonradiative Transitions in Nitro-Polycyclic Aromatic Hydrocarbons: Excited-State Dynamics in 1-Nitronaphthalene. *J. Chem. Phys.* **2009**, *131*, 224518
- (33) Yang, C.; Su, H.; Sun, X.; George, M. W. Ultrafast Formation of the Benzoic Acid Triplet upon Ultraviolet Photolysis and its Sequential Photodissociation in Solution. *J. Chem. Phys.* **2012**, *136*, 204507
- (34) Parker, D. S. N.; Minns, R. S.; Penfold, T. J.; Worth, G. A.; Fielding, H. H. Ultrafast Dynamics of the S_1 Excited State of Benzene. *Chem. Phys. Lett.* **2009**, *469*, 43 – 47.
- (35) Penfold, T. J.; Worth, G. A. The Effect of Molecular Distortions on Spin-Orbit Coupling in Simple Hydrocarbons. *Chem. Phys.* **2010**, *375*, 58 – 66.
- (36) Etinski, M.; Tatchen, J.; Marian, C. M. Time-Dependent Approaches for the Calculation of Intersystem Crossing Rates. *J. Chem. Phys.* **2012**, *134*, 154105.
- (37) Richter, M.; Marquetand, P.; González-Vázquez, J.; Sola, I.; González, L. SHARC: Ab Initio Molecular Dynamics with Surface Hopping in the Adiabatic Representation Including Arbitrary Couplings. *J. Chem. Theory Comput.* **2011**, *7*, 1253–1258.

- (38) Marquetand, P.; Richter, M.; González-Vázquez, J.; Sola, I.; González, L. Nonadiabatic Ab Initio Molecular Dynamics Including Spin-Orbit Coupling and Laser Fields. *Faraday Discuss.* **2011**, *153*, 261–273.
- (39) Bajo, J. J.; González-Vázquez, J.; Sola, I. R.; Santamaria, J.; Richter, M.; Marquetand, P.; González, L. Mixed Quantum-Classical Dynamics in the Adiabatic Representation to Simulate Molecules Driven by Strong Laser Pulses. *J. Phys. Chem. A* **2012**, *116*, 2800–2807.
- (40) Barker, D. L.; Marsh, R. E. The Crystal Structure of Cytosine. *Acta Crystallogr.* **1964**, *17*, 1581–1587.
- (41) Blancafort, L.; Bearpark, M. J.; Robb, M. A. Computational Modeling of Cytosine Photophysics and Photochemistry: From the Gas Phase to DNA. In Shukla, M. K.; Leszczynski, J. eds. *Radiation Induced Molecular Phenomena in Nucleic Acids* (Springer Netherlands), vol. 5 of *Challenges and Advances in Computational Chemistry and Physics* **2008** pp. 473–492.
- (42) Matsika, S.; Zhou, C.; Kotur, M.; Weinacht, T. C. Combining Dissociative Ionization Pump-Probe Spectroscopy and Ab Initio Calculations to Interpret Dynamics and Control Through Conical Intersections. *Faraday Discuss.* **2011**, *153*, 247–260.
- (43) Ismail, N.; Blancafort, L.; Olivucci, M.; Kohler, B.; Robb, M. A. Ultrafast Decay of Electronically Excited Singlet Cytosine via a π, π^* to n_o, π^* State Switch. *J. Am. Chem. Soc.* **2002**, *124*, 6818–6819.
- (44) Merchán, M.; Serrano-Andrés, L. Ultrafast Internal Conversion of Excited Cytosine via the Lowest $\pi\pi^*$ Electronic Singlet State. *J. Am. Chem. Soc.* **2003**, *125*, 8108–8109.
- (45) Tomić, K.; Tatchen, J.; Marian, C. M. Quantum Chemical Investigation of the Electronic Spectra of the Keto, Enol, and Keto-Imine Tautomers of Cytosine. *J. Phys. Chem. A* **2005**, *109*, 8410–8418.
- (46) Blancafort, L.; Bertran, J.; Sodupe, M. Triplet (π, π^*) Reactivity of the Guanine-Cytosine DNA Base Pair: Benign Deactivation versus Double Tautomerization via Intermolecular Hydrogen Transfer. *J. Am. Chem. Soc.* **2004**, *126*, 12770–12771.
- (47) Blancafort, L. Energetics of Cytosine Singlet Excited-State Decay Paths - a Difficult Case for CASSCF and CASPT2. *Photochem. Photobiol.* **2007**, *83*, 603–610.
- (48) Kotur, M.; Weinacht, T. C.; Zhou, C.; Kistler, K. A.; Matsika, S. Distinguishing Between Relaxation Pathways by Combining Dissociative Ionization Pump Probe Spectroscopy and Ab Initio Calculations: A Case Study of Cytosine. *J. Chem. Phys.* **2011**, *134*, 184309.
- (49) Blancafort, L.; Robb, M. A. Key Role of a Threefold State Crossing in the Ultrafast Decay of Electronically Excited Cytosine. *J. Phys. Chem. A* **2004**, *108*, 10609–10614.
- (50) Kistler, K. A.; Matsika, S. Radiationless Decay Mechanism of Cytosine: An Ab Initio Study with Comparisons to the Fluorescent Analogue 5-Methyl-2-Pyrimidinone. *J. Phys. Chem. A* **2007**, *111*, 2650–2661.
- (51) Kistler, K. A.; Matsika, S. Three-State Conical Intersections in Cytosine and Pyrimidinone Bases. *J. Chem. Phys.* **2008**, *128*, 215102.
- (52) Hudock, H. R.; Martínez, T. J. Excited-State Dynamics of Cytosine Reveal Multiple Intrinsic Subpicosecond Pathways. *Chem. Phys. Chem.* **2008**, *9*, 2486–2490.
- (53) González-Vázquez, J.; González, L. A Time-Dependent Picture of the Ultrafast Deactivation of Keto-Cytosine Including Three-State Conical Intersections. *Chem. Phys. Chem.* **2010**, *11*, 3617–3624.

- (54) Barbatti, M.; Aquino, A. J. A.; Szymczak, J. J.; Nachtigallova, D.; Lischka, H. Photodynamical Simulations of Cytosine: Characterization of the Ultrafast Bi-Exponential UV Deactivation. *Phys. Chem. Chem. Phys.* **2011**, *13*, 6145–6155.
- (55) Merchán, M.; Serrano-Andrés, L.; Robb, M. A.; Blancafort, L. Triplet-State Formation Along the Ultrafast Decay of Excited Singlet Cytosine. *J. Am. Chem. Soc.* **2005**, *127*, 1820–1825.
- (56) González-Luque, R.; Climent, T.; González-Ramírez, I.; Merchán, M.; Serrano-Andrés, L. Singlet-Triplet States Interaction Regions in DNA/RNA Nucleobase Hypersurfaces. *J. Chem. Theory. Comput.* **2010**, *6*, 2103–2114.
- (57) Werner, H. J.; Knowles, P. J. A Second Order Multiconfiguration SCF Procedure with Optimum Convergence. *J. Chem. Phys.* **1985**, *82*, 5053–5063.
- (58) Knowles, P. J.; Werner, H. J. An Efficient Second-Order MC SCF Method for Long Configuration Expansions. *Chem. Phys. Lett.* **1985**, *115*, 259 – 267.
- (59) Kosma, K.; Schröter, C.; Samoylova, E.; Hertel, I. V.; Schultz, T. Excited-State Dynamics of Cytosine Tautomers. *J. Am. Chem. Soc.* **2009**, *131*, 16939–16943.
- (60) Ho, J.-W.; Yen, H.-C.; Chou, W.-K.; Weng, C.-N.; Cheng, L.-H.; Shi, H.-Q.; Lai, S.-H.; Cheng, P.-Y. Disentangling Intrinsic Ultrafast Excited-State Dynamics of Cytosine Tautomers. *J. Phys. Chem. A* **2011**, *115*, 8406–8418.
- (61) Pecourt, J. M. L.; Peon, J.; Kohler, B. DNA Excited-State Dynamics: Ultrafast Internal Conversion and Vibrational Cooling in a Series of Nucleosides. *J. Am. Chem. Soc.* **2001**, *123*, 10370–10378.
- (62) Kotur, M.; Weinacht, T.; Zhou, C.; Matsika, S. Following Ultrafast Radiationless Relaxation Dynamics with Strong Field Dissociative Ionization: A Comparison Between Adenine, Uracil, and Cytosine. *IEEE J. Sel. Top. Quantum El.* **2012**, *18*, 187 –194.
- (63) Martínez-Fernández, L.; González, L.; Corral, I. An Ab Initio Mechanism for Efficient Population of Triplet States in Cytotoxic Sulfur Substituted DNA Bases: The Case of 6-Thioguanine. *Chem. Commun.* **2012**, *48*, 2134–2136.
- (64) Lower, S. K.; El-Sayed, M. A. The Triplet State and Molecular Electronic Processes in Organic Molecules. *Chem. Rev.* **1966**, *66*, 199–241.
- (65) Braslavsky, S. E. Glossary of Terms Used in Photochemistry, 3rd edition (IUPAC recommendations 2006). *Pure Appl. Chem.* **2007**, *79*, 293–465.
- (66) Marian, C. M. Spin-Orbit Coupling and Intersystem Crossing in Molecules. *WIREs Comput. Mol. Sci.* **2012**, *2*, 187 – 203.
- (67) Chergui, M. On the Interplay Between Charge, Spin and Structural Dynamics in Transition Metal Complexes. *Dalton Trans.* **2012**.

Femtosecond Intersystem Crossing in the DNA Nucleobase Cytosine

Supporting Information

I. Computational details regarding dynamical simulations and initial conditions

The simulation of the deactivation dynamics of keto-cytosine in gas phase was performed using the semiclassical SHARC method¹ that calculates non-adiabatic molecular dynamics simulations using Tully’s fewest switches criterion.² The nuclei are treated as classical point charges that obey Newton’s equations of motion.³ To follow the trajectory of the nuclei, the Velocity-Verlet algorithm⁴ was applied with a time step of 0.5 fs. The energy gradients that serve as an input for the Velocity-Verlet algorithm were analytically calculated in the electronic part of the simulation. In contrast to the nuclei, the electrons are treated by means of ab initio quantum mechanics. Here, the electronic wave function is expanded into a linear combination of basis functions, that represent the contribution of the different calculated electronic states to the total wave function. The time evolution of the quantum amplitudes is followed using the 5th order Butcher algorithm⁵ with a time step of $5 \cdot 10^{-6}$ fs. The resulting values were corrected for decoherence effects using the method of Granucci and Persico with a parameter of $\alpha = 0.1$ hartree.⁶

Initial conditions for the trajectories are generated with a Wigner harmonic distribution of 5000 uncorrelated geometries and velocities. For this purpose, the equilibrium geometry was optimized and normal modes were calculated with the TURBOMOLE package,^{7,8} the B3LYP hybrid functional^{9,10} and the TZVP basis set.¹¹ For each of the initial conditions, a single-point calculation employing the Complete Active Space Self-Consistent-Field approach^{12,13} averaged over four singlet states with the MOLPRO¹⁴ package and the 6-31G* basis set was done (see Section III for further electronic structure details). All 5000 initial conditions and their calculated oscillator strengths and vertical

excitations were used to create a UV absorption spectrum as described in Ref.¹⁵ The spectrum, see Fig. S1, is in good agreement with that previously published in Ref.¹⁶

Using Newton-X^{17,18} it is possible to estimate the instantaneous probability to excite keto-cytosine at every geometry to a particular excited state. Applying these probabilities to the calculated 5000 initial conditions, we obtain 591 trajectories starting from the S_1 , 685 starting from the S_2 and 192 starting from the S_3 state. Since the molecular dynamics simulations converge with notably less than 1468 trajectories, only 150 trajectories have been propagated. This ensemble consisted of 60, 70 and 20 trajectories, starting from the S_1 , S_2 and S_3 respectively. The results were statistically evaluated for all trajectories and checked for convergence. Each trajectory was propagated during 1 ps using time steps of 0.5 fs.

Population transfer of the semiclassical trajectories between the different electronic states was calculated according to the Tully’s fewest switches criterion² in the adiabatic representation, including non-adiabatic couplings as well as spin-orbit couplings. In order to avoid unphysical hops and for computational reasons, the hopping probabilities were only calculated for states that, after a hop, would lead to an increase of potential energy of 1 eV or less. After a hop, the kinetic energy was adjusted in order to conserve the total energy of the system. Therefore, the velocities (i.e. the kinetic energies) of the atoms were scaled along their current direction in order to keep the total energy constant.

If a trajectory populated the S_0 state for at least 20 fs with a coefficient greater than 0.99, it was stopped automatically and it was assumed that the population in the S_0 remains constant for the rest of the simulation.

II. Deactivation pathways with an excitation bandwidth of 4.75 ± 0.25 eV

Figure S2 displays the time evolution of all the state populations when limiting the excitation

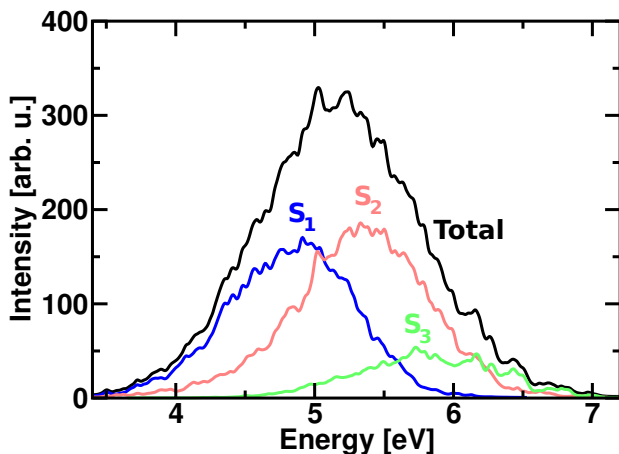


Figure S1: UV absorption spectrum of keto-cytosine.

bandwidth to 4.75 ± 0.25 eV, in accord to the energy range corresponding to the experiments, see e.g. Ref. ¹⁹ In this energy range only 42 trajectories are considered. As it can be seen the results are qualitatively the same as those shown in Fig. 1 of the manuscript using 150 trajectories in the broader energy range of 4 to 7 eV. After 1000 fs the populations are converged to the same ratio, about 90% in S_0 and 10% in T_1 . Moreover, the S_0 gains about 40% population within 10-15 fs. Obviously, the initial distribution of the trajectories is changed with respect to the full picture with 150 trajectories: The S_1 is now the strongest populated state in the beginning, while S_2 and S_3 states are less populated and therefore hit zero population faster. However, the early population of the triplet states and the deactivation channels, and therefore, the main conclusions discussed in the main text are the same as in the broader range. The reason why the two sets of energy ranges give very similar dynamical results is based on the fact that the S_1 state provides the most important channel for the ultrafast ISC observed in our simulations. The branching between the two main deactivation pathways from S_1 (i.e. ISC towards T_2 and following IC towards T_1 or IC from S_1 to S_0) is similar in the complete range of initial conditions. Then, because S_1 and T_2 are nearly degenerate for many geometries, the smaller excess energy of the trajectories with limited excitation bandwidth does not influence the efficiency of the ISC channel.

Thus, the early population of the triplet states and the deactivation channels discussed in the main text are almost independent of the excitation energy range.

The deactivation pathways visualized in Fig. 2 are based on the number of surface hops that occurred between the different pairs of states in the molecular dynamics simulations. Since jumps can take place in two directions, the net amount of hops for a pair of states i and j can be calculated by subtracting the number of hops from state i to j from the number of hops from j to i . The temporal evolution of this quantity is shown in Fig. S3. Panel a) depicts the pathways for internal conversion (IC) between the singlet states, panel b) the intersystem crossing (ISC) pathways between singlet and triplet states and panel c) the IC between the triplets. The curves can be fitted with exponential functions according to $N_i(1 - e^{-t/\tau_i})$ in order to get time constants τ_i for the respective pathways. These time constants are collected in Table S1 and are consistent with all the available data. However, due to the sensitivity of the time constants with the energy and the lack of dynamical correlation in the electronic structure calculations, they should be regarded as qualitative.

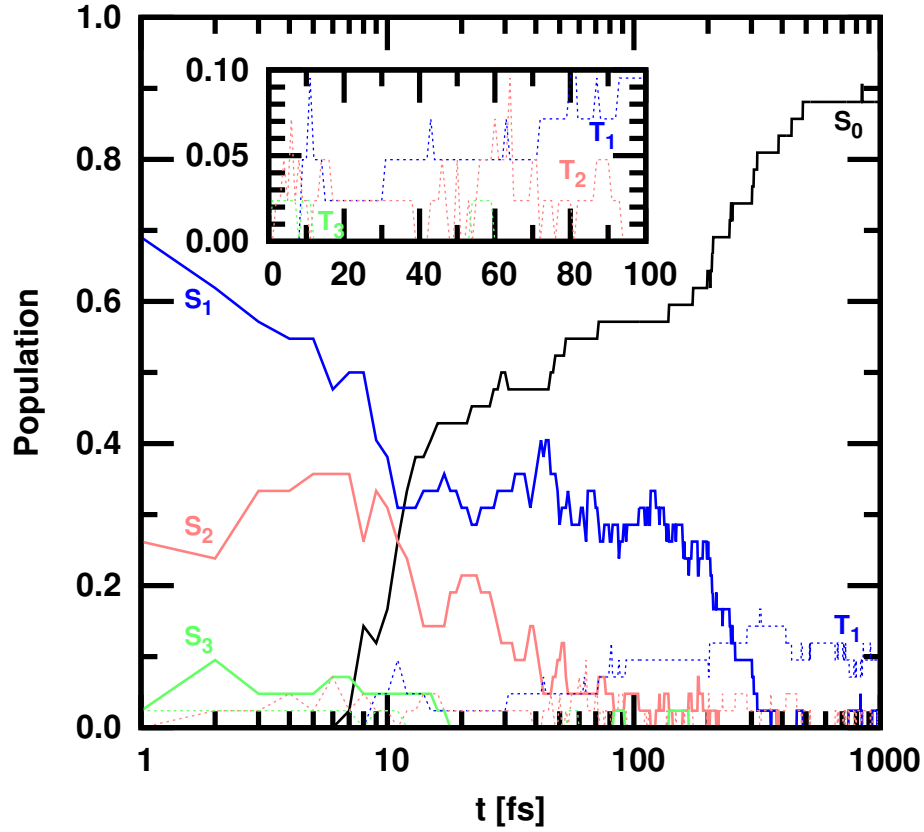


Figure S2: Time evolution of the singlet (solid) and triplet (dotted) states during the first picosecond. The inset zooms the first 100 fs. The S_0 ground state population is in black, S_1/T_1 states populations are in red, S_2/T_2 in blue and S_3/T_3 in green. Excitation bandwidth is limited to 4.75 ± 0.25 eV.

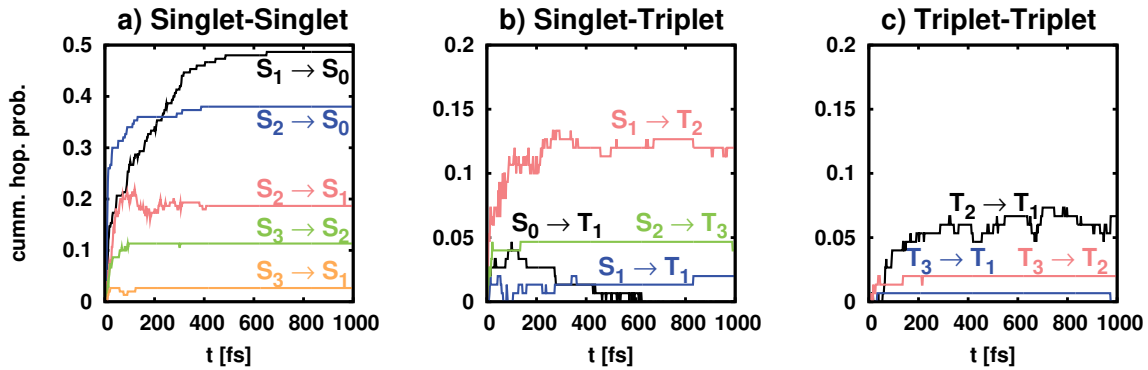


Figure S3: Net hops accumulated in time.

Table S1: Time constants fitted to accumulated hopping probability curves (see Fig. S2)

Pathway	time constant	Error [%]
$S_1 \rightarrow S_0$	$\tau_1 = 155$ fs	1
$S_2 \rightarrow S_0$	$\tau_2 = 25$ fs	2
$S_2 \rightarrow S_1$	$\tau_3 = 25$ fs	3
$S_3 \rightarrow S_1$	$\tau_4 = 109$ fs	3
$S_3 \rightarrow S_2$	$\tau_5 = 22$ fs	2
$S_1 \rightarrow T_1$	$\tau_6 = 1000$ fs	>100
$S_1 \rightarrow T_2$	$\tau_7 = 78$ fs	2
$S_2 \rightarrow T_3$	$\tau_8 = 14$ fs	4
$T_2 \rightarrow T_1$	$\tau_4 = 216$ fs	3
$T_3 \rightarrow T_1$	$\tau_5 = 33$ fs	2
$T_3 \rightarrow T_2$	$\tau_5 = 82$ fs	2

III. Ab initio quantum chemical calculations

At each time step of the propagation, the electronic states of keto-cytosine and corresponding electronic properties have been calculated using the state-average SA7-CAS(12,9)/6-31G* level of theory using 12 electrons distributed in 9 orbitals, as implemented in the MOLPRO software package.¹⁴ As in Ref.,¹⁶ the active space consists of 4 π , 3 π^* and 2 n orbitals, see Fig. S4. Seven states (four singlets and three triplets) are averaged with equal weights. Relativistic corrections were taken into account by the use of the 2nd order Douglas-Kroll-Hess Hamiltonian.^{20,21}

Table S2 shows the vertical excitation energies of the lowest-lying three singlet and triplet excited states at the equilibrium geometry obtained at SA7-CASSCF(12,9)/6-31G*/B3LYP/TZVP level of theory as well

as other levels of theory for comparison, obtained using MOLCAS 7.6.²²⁻²⁴ As it can be seen, the energies are rather sensitive to the introduction of dynamical correlation and also to the optimized geometry employed. The values obtained with SA7-CASSCF(12,9)/6-31G*/B3LYP/TZVP are similar to those obtained when calculating the singlets and triplet states separately (SA4+SA3). The energy of the lowest singlet state S_1 , which determines the maximum of the first UV absorption band, is decreased when perturbation theory is included (MS-CASPT2/SA7-CASSCF(12,9)/6-31G*/B3LYP/TZVP).

At MP2 level of theory the ground state equilibrium structure gets slightly pyramidalized at the NH_2 group while B3LYP keeps the molecule completely planar. This geometrical difference is not relevant in the ab initio MD simulations, since an ensemble of geometries sampled over all the degrees of freedom according to the ZPE is considered. However, as it can be seen in Table S2, the out of plane deformation is important to obtain an energy closer to the experimental S_1 -origin in the gas phase^{25,26} located at ca. 4.7 eV. The MS-CASPT2 value for the S_1 using SA4+SA3-CAS(12,9)/6-31G*/MP2/6-31G* level of theory is predicted at 4.8 eV, very close to the experimental one. A similar value is also obtained using DFT-MRCI calculations.²⁷

Since MS-CASPT2 trajectories are computationally not affordable and electronic couplings are not available at DFT-MRCI level of theory, our calculations were done using SA7-CAS(12,9)/6-31G*/B3LYP/TZVP. The obtained vertical excitation energies are in agreement with those previously reported also at the CAS/6-31G** level of theory by Merchán and coworkers.²⁸

References

- (1) Richter, M.; Marquetand, P.; González-Vázquez, J.; Sola, I.; González, L. SHARC: Ab Initio Molecular Dynamics with Surface Hopping in the Adiabatic Representation Including Arbitrary Couplings. J.

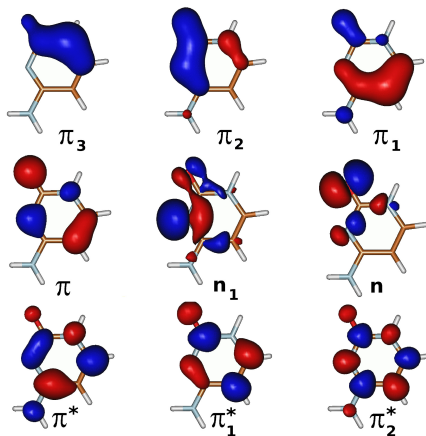


Figure S4: Orbitals included in the SA7-CASSCF(12,9)/6-31G* calculations.

Table S2: Vertical excitation energies of keto-cytosine at the equilibrium geometry computed at different levels of theory, as specified. Oscillator strengths are given in parentheses.

<i>ab initio</i> methodology	S ₁	S ₂	S ₃	T ₁	T ₂	T ₃
SA7-CAS(12,9)/6-31G**/B3LYP/TZVP	5.37 (0.081)	5.38 (0.002)	5.79 (0.002)	3.81	5.14	5.17
SA4+SA3-CAS(12,9)/6-31G**/B3LYP/ZVP	5.26 (0.083)	5.41 (0.001)	5.72 (0.004)	3.80	4.96	5.02
MS-CASPT2 using previous one	5.00 (0.073)	5.37 (0.002)	5.81 (0.002)	4.15	5.17	5.29
SA7-CAS(12,9)/6-31G**/MP2/6-31G*	5.08 (0.074)	5.09 (0.000)	5.46 (0.005)	3.54	4.91	4.93
SA4+SA3-CAS(12,9)/6-31G**/MP2/6-31G*	4.98 (0.080)	5.10 (0.001)	5.45 (0.004)	3.48	4.74	4.77
MS-CASPT2 using previous one	4.80 (0.072)	5.15 (0.002)	5.61 (0.002)	3.96	4.90	5.17
CAS(12,9)/6-31G** Ref ²⁸	5.32	5.34	5.67	3.72	5.01	5.19
MS-CASPT2 Ref ²⁸	4.53 (0.065)	5.04 (0.001)	5.11 (0.003)	3.65	4.68	4.77
DFT-MRCI//B3LYP/TZVP Ref ²⁷	4.83 (0.080)	5.02 (0.002)	5.50 (0.001)			

- Chem. Theory. Comput. **2011**, 7, 1253–1258.
- (2) Tully, J. C. Molecular Dynamics with Electronic Transitions. J. Chem. Phys. **1990**, 93, 1061–1071.
 - (3) Newton, I. *Philosophiae Naturalis Principia Mathematica* **1726** (Harvard Univ. Press, Cambridge).
 - (4) Verlet, L. Computer “Experiments” on Classical Fluids. II. Equilibrium Correlation Functions. Phys. Rev. **1968**, 165, 201–214.
 - (5) Butcher, J. A Modified Multistep Method for the Numerical Integration of Ordinary Differential Equations. J. Assoc. Comput. Mach. **1965**, 12, 124–135.
 - (6) Granucci, G.; Persico, M. Critical Appraisal of the Fewest Switching Algorithm for Surface Hopping. J. Chem. Phys. **2007**, 126, 134114.
 - (7) Ahlrichs, R.; Bär, M.; Häser, M.; Horn, H.; Kölmel, C. Electronic Structure Calculations on Workstation Computers: The Program System Turbomole. Chem. Phys. Lett. **1989**, 162, 165–169.
 - (8) Treutler, O.; Ahlrichs, R. Efficient Molecular Numerical Integration Schemes. J. Chem. Phys. **1995**, 102, 346–354.
 - (9) Becke, A. D. Density-Functional Thermochemistry. III. The Role of Exact Exchange. J. Chem. Phys. **1993**, 98, 5648–5652.
 - (10) Lee, C.; Yang, W.; Parr, R. G. LYP Correlation: Development of the Colle-Salvetti

- Correlation-Energy Formula into a Functional of the Electron Density. Phys. Rev. B **1988**, 37, 785.
- (11) Schäfer, A.; Huber, C.; Ahlrichs, R. Fully Optimized Contracted Gaussian Basis Sets of Triple Zeta Valence Quality for Atoms Li to Kr. J. Chem. Phys. **1994**, 100, 5829–5835.
- (12) Werner, H. J.; Knowles, P. J. A Second Order Multiconfiguration SCF Procedure with Optimum Convergence. J. Chem. Phys. **1985**, 82, 5053–5063.
- (13) Knowles, P. J.; Werner, H. J. An Efficient Second-Order MCSCF Method for Long Configuration Expansions. Chem. Phys. Lett. **1985**, 115, 259 – 267.
- (14) Werner, H. J.; Knowles P. J.; Lindh, R.; Manby, F. R.; Schütz M.; Celani, P.; Korona, T.; Mitrushenkov, A.; Rauhut, G.; Adler, T. B. et al. MOLPRO, Version 2010.1, a Package of Ab Initio Programs.
- (15) Barbatti, M.; Aquino, A. J. A.; Lischka, H. The UV Absorption of Nucleobases: Semi-Classical Ab Initio Spectra Simulations. Phys. Chem. Chem. Phys. **2010**, 12, 4959–4967.
- (16) González-Vázquez, J.; González, L. A Time-dependent Picture of the Ultrafast Deactivation of Keto-Cytosine Including Three-State Conical Intersections. Chem. Phys. Chem. **2010**, 11, 3617–3624.
- (17) Barbatti, M.; Granucci G.; Persico, M.; Ruckebauer, M.; Vazdar, M.; Eckert-Maksić, M.; Lischka, H. The On-The-Fly Surface-Hopping Program System Newton-X: Application to Ab Initio Simulation of the Nonadiabatic Photodynamics of Benchmark Systems. J. Photochem. Photobiol. A **2007**, 190, 228–240.
- (18) Barbatti, M.; Granucci, G.; M. Ruckebauer, J. P.; Persico, M.; Lischka, H. Newton-X: A Package for Newtonian Dynamics Close to the Crossing Seam **2007**, www.newtonx.org.
- (19) Kosma, K.; Schröter, C.; Samoylova, E.; Hertel, I. V.; Schultz, T. Excited-State Dynamics of Cytosine Tautomers. J. Am. Chem. Soc. **2009**, 131, 16939–16943.
- (20) Douglas, M.; Kroll, N. M. Quantum Electrodynamical Corrections to the Finestructure of Helium. Ann. Phys. **1974**, 82, 89–155.
- (21) Hess, B. A. Relativistic Electronic-Structure Calculations Employing a Two-Component No-Pair Formalism with External-Field Projection Operators. Phys. Rev. A **1986**, 33, 3742–3748.
- (22) Aquilante, F.; Vico, L. D.; Ferré, N.; Ghigo, G.; Malmqvist, P.-Å; Neogrády, P.; Pedersen, T. B.; Pitonak, M.; Reiher, M.; Roos, B. O. et al. MOLCAS 7: The Next Generation. J. Comp. Chem. **2010**, 31, 224–247.
- (23) Veryazov, V.; Widmark, P.; Serrano-Andrés, L.; Lindh, R.; Roos, B. O. MOLCAS as a Development Platform for Quantum Chemistry Software. Int. J. Quantum Chem. **2004**, 100, 626635.
- (24) Karlström, G.; Lindh, R.; Malmqvist, P.-Å; Roos, B. O.; Ryde, U.; Veryazov, V.; Widmark, P.-O.; Cossi, M.; Schimelpfennig, M.; Neogrády, P.; Seijo, L. MOLCAS: A Program Package for Computational Chemistry. Comp. Mater. Sci. **2003**, 28, 222–239.
- (25) Nir, E.; Müller, M.; Grace, L.; de Vries, M. Rempy Spectroscopy of Cytosine. Chem. Phys. Lett. **2002**, 355, 59 – 64.
- (26) Nir, E.; Plützer, C.; Kleinermanns, K.; de Vries, M. Properties of Isolated DNA Bases, Base Pairs and Nucleosides Examined by Laser Spectroscopy. Euro. Phys. J. D **2002**, 20, 317–329.
- (27) Tomić, K.; Tatchen, J.; Marian, C. M. Quantum Chemical Investigation of the Electronic Spectra of the Keto, Enol, and Keto-Imine Tautomers of Cytosine. J. Phys. Chem. A **2005**, 109, 8410–8418.

- (28) Merchán, M.; Serrano-Andrés, L.; Robb, M. A.; Blancafort, L. Triplet-State Formation Along the Ultrafast Decay of Excited Singlet Cytosine. J. Am. Chem. Soc. **2005**, 127, 1820–1825.